

FSM: correspondenceless scan-matching of panoramic 2D range scans

Alexandros Filotheou, Georgios D. Sergiadis, Antonis G. Dimitriou

Abstract—Recent years have seen the introduction of more affordable but less accurate 2D range sensors whose field of view is 2π . Scan-matching with these has been insufficiently researched, while being a challenge due to these sensors’ increased measurement uncertainty. This paper proposes a real-time method for matching scans extracted from panoramic 2D LIDAR sensors. The method leverages properties of the Fourier transform which arise due to the periodicity of the range signal. Matching is performed in a correspondenceless manner. The proposed method outperforms established scan-matching methods in terms of pose accuracy and robustness in tests on public domain data, and over noise levels of commercially available sensors. The source code is available for download.

Index Terms—Scan-matching, localisation, panoramic LIDAR

I. INTRODUCTION

Consider a robot capable of motion, equipped with a Light Detection and Ranging sensor (LIDAR), capturing a measurement \mathcal{S}_0 at time t_0 from pose p_0 in some reference frame. The robot then moves to pose p_1 at time t_1 at which time it captures measurement \mathcal{S}_1 . Provided overlap between the two scans, estimating the rigid-body transformation \mathbf{T} that projects the endpoints of \mathcal{S}_1 to those of \mathcal{S}_0 with the least error is known as scan-matching. The solution to the scan-matching problem is central to methods of Localisation [1], Navigation [2], and Simultaneous Localisation and Mapping (SLAM) [3][4], as \mathbf{T} is the rigid-body transformation $p_1 - p_0$: i.e. the solution to scan-matching provides localisation information at time t_1 , relative to p_0 . For this reason, along with the high measurement accuracy of LIDAR sensors, scan-matching is also used as a means to improving, providing, or substituting odometric measurements (where available; fig. 1), as the latter are prone to unbounded and unpredictable tire and wheel slippage [5][6].

LIDAR sensors with a field of view of 360° , i.e. panoramic sensors, were for years constrained to high price ranges, and most provided 3D measurements. Therefore research on scan-matching with 2D LIDAR sensors mostly focused on non-panoramic sensors, with scan matching methods being used without distinction with regard to field of view. In recent years, however, price-appealing 2D LIDAR sensors have emerged, but at the cost of increased measurement uncertainty. The introduction of these sensors warrants targeted research into scan-matching with the use of panoramic

This work was supported by the European Union and Greek National Funds through the Operational Program Competitiveness, Entrepreneurship, and Innovation, under the call Research Create Innovate under Project T2EDK-02000. Corresponding author: Alexandros Filotheou, alefilot@auth.gr. The authors are with the Department of Electrical and Computer Engineering, Aristotle University of Thessaloniki, 54124 Thessaloniki, Greece

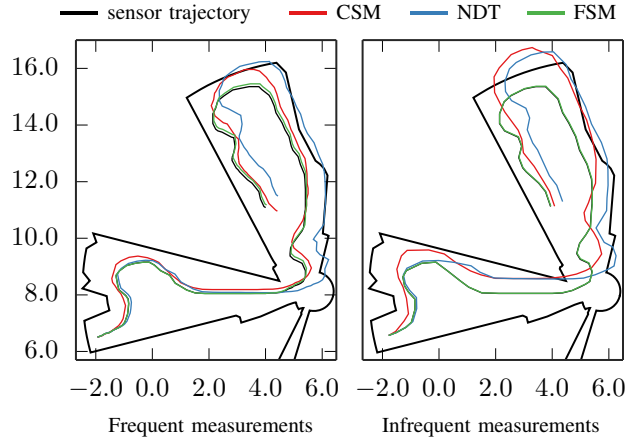


Fig. 1: Scan-matching as “laser odometry”: the robot moves from the lower left portion of the environment to the upper right, capturing 2D range scans along its trajectory. The coloured routes show the estimated path of the robot derived from each method. The proposed method’s error is invariant to angular and locational displacement

LIDAR sensors, due to (a) the afforded periodicity of the range signal, and (b) the need of addressing the high levels of measurement noise with regard to the transformation errors of current scan-matching algorithms.

This paper introduces a real-time method specifically targeting the matching of 2D panoramic range scans. Its errors are largely invariant to angular and locational displacement for a given level of measurement noise. The central contributions of the paper are:

- To the best of the author’s knowledge, the first method explicitly addressing the matching of panoramic 2D range scans that operates without establishing correspondences between input scans
- The extrication from the need of a prior transformation estimate
- The introduction of a method that aims at reducing the orientation error to lower than the sensor’s angle increment compared to relevant prior work
- The parameter set needed by the proposed method is intuitive, smaller than those of established methods, and trades accuracy for execution time
- The thorough evaluation of the proposed method against five established scan-matching algorithms in common use, with benchmark datasets, using measurement noise levels from common-use, commercially available sensors

The rest of the paper is structured as follows. In section II

necessary notions are defined, and the problem of matching panoramic 2D range scans is formulated. A brief review of methods matching 2D range scans is given in section III. Section IV provides an analysis of the proposed method. The experimental setup and are illustrated in section V. Section VI concludes this paper.

II. DEFINITIONS AND PROBLEM FORMULATION

Definition I. *Definition of a range scan captured from a conventional 2D LIDAR sensor.* A conventional 2D LIDAR sensor provides a finite number of ranges, i.e. distances to objects within its range, on a horizontal cross-section of its environment, at regular angular and temporal intervals, over a defined angular range [7]. A range scan \mathcal{S} , consisting of N_s rays over an angular range λ , is an ordered map $\mathcal{S} : \Theta \rightarrow \mathbb{R}_{\geq 0}$, $\Theta = \{\theta_n \in [-\frac{\lambda}{2}, +\frac{\lambda}{2}) : \theta_n = -\frac{\lambda}{2} + \lambda \frac{n}{N_s}, n = 0, 1, \dots, N_s - 1\}$. Angles θ_n are expressed relative to the sensor's heading, in the sensor's frame of reference. The angular distance between two consecutive rays is the sensor's angle increment $\gamma \triangleq \lambda/N_s$.

Definition II. *Definition of a map-scan.* A map-scan is a virtual scan that encapsulates the same pieces of information as a scan derived from a physical sensor. Only their underlying operating principle is different due to the fact the map-scan refers to distances to the boundaries of a point-set, referred to as the map, rather than within a real environment. A map-scan is derived by means of locating intersections of rays emanating from the estimate of the sensor's pose estimate and the boundaries of the map.

Problem I. Let a mobile robot, capable of motion in the $x-y$ plane, be equipped with a coplanarly mounted range scan sensor emitting N_s rays. Let also the following be available or standing:

- The angular range of the range sensor is 360°
- A 2D range scan \mathcal{S}_0 , captured at time t_0
- A 2D range scan \mathcal{S}_1 , captured at $t_1 > t_0$

Then the objective is estimating the 3D rigid-body transformation $\mathbf{T} = (\Delta x, \Delta y, \Delta\theta)$ which, when applied to the endpoints of \mathcal{S}_1 , aligns them to those of \mathcal{S}_0 with the least error. Equivalently, roto-translation \mathbf{T} corresponds to the relative motion of the sensor from the pose where it captured \mathcal{S}_0 to the pose from which it captured \mathcal{S}_1 .

III. PRIOR WORK

Scan-matching with the use of a 2D LIDAR sensor began with Iterative Dual Correspondences (IDC) [8], an algorithm incorporating elements of the Iterative Closest Point (ICP) algorithm [9]. The latter and its variants, e.g. [10]-[14], have become the de facto scan-matching algorithms in 2D and 3D settings, with research using ICP being still ongoing [15]-[21]. In particular, PL-ICP [22] has been widely adopted due to its increased accuracy among ICP variants, and the availability of its source code. ICP and its variants, however, exhibit varying performance [23], limited by the noise level in the input scans, the choice of prior, and the configuration

of the parameters governing their response. The vast majority of all matching methods adopt ICP's approach of establishing correspondences between the two input scans, using various mechanisms, assumptions, and types of sources (e.g. features instead of points; a detailed review of scan-matching methods may be found in [29]). The major problem with establishing correspondences is that the process becomes more inefficient and error-prone as measurement noise increases.

By contrast, the method introduced in this paper does not operate by establishing correspondences. Its rotational component is most akin to those of [26] and [27]. They use Phase-Only Matched Filtering (POMF) [28] in both rotation and translation components; the former in one dimension and the latter in two dimensions. In the latter, the requirements for a real-time solution and adequate accuracy cannot be fulfilled simultaneously due to the inability to balance high grid resolution (and therefore high accuracy) with regular sensor updates. The former alleviates this limitation by operating in one dimension, but suffers from the same causes, namely, discretisation errors. Whereas the latter is dependent on the grid's resolution, the former is dependent on the sensor's immutable angle increment. In both methods, both the rotational and translational components are affected, but no mitigation technique is employed to decrease the errors of either their components. By contrast, the method introduced in this paper addresses all the above issues by (a) aiming to extricate the orientation error from the sensor's angle increment, (b) employing a continuous-space translation method, and (c) fulfilling the real-timeliness constraint.

IV. APPROACH

Problem I is iteratively decomposed into two disjunctive sub-problems. The first is estimating the relative orientation of \mathcal{S}_1 with respect to \mathcal{S}_0 under the assumption that both are captured from the same location (subsection IV-A). In order to do so, \mathcal{S}_0 is first transformed into a point-set (the map) by projection to the 2D plane. A number of map-scans are then captured from the projection origin, at consecutive angular intervals. The intervals' sizes are smaller than the sensor's angle increment in order for the magnitude of the angular approximation error to be lower than the angle increment. The map-scans are then compared against \mathcal{S}_1 for similarity in the POMF matching sense. The output is an orientation difference estimate between each map-scan and \mathcal{S}_1 . In order to increase discernibility between the least erroneous orientation estimate and the other estimates, the pose estimate is updated with each orientation estimate, and given over to the translation correction system, whose resulting location error is proportional to the poses's orientation error, for one iteration. The similarity between map-scans captured from these estimates within the map and \mathcal{S}_1 is captured in a per-ray range error metric. The final orientation estimate of \mathcal{S}_1 is that of the pose estimate whose map-scan scores the lowest error according to this metric.

The second sub-problem is estimating the relative translational displacement of \mathcal{S}_1 with respect to \mathcal{S}_0 under the assumption that both are captured from poses of the same

orientation (subsection IV-B). The solution is given via scan-to-map-scan matching by transforming \mathcal{S}_0 to a point-set and matching map-scans, derived from the pose estimate of \mathcal{S}_1 within the point-set, to \mathcal{S}_1 itself. The matching between the two is derived from first principles given the scans' periodicity and homorrientedness; it is facilitated by iteratively updating the position estimate by a vector which is a function of the first term of the DFT of the difference between \mathcal{S}_1 and map-scans derived from the point-set of \mathcal{S}_0 [30].

The solution to the first sub-problem is followed by that to the second sub-problem. This process is iterated until termination conditions are met. Subsection IV-C presents the method of how these two are woven together into the system that solves Problem I that is proposed in this work.

A. Estimation of Relative Orientation

Let the assumptions of Problem I be standing. Assume that the two scans were captured from the same location but from different orientations. Denoting with $\mathcal{F}\{\mathcal{S}\}$ the Discrete Fourier Transform (DFT) of signal \mathcal{S} , with $\mathcal{F}^{-1}\{\mathcal{S}\}$ its inverse, with c^* the conjugate of complex c , and with $|c|$ its magnitude, calculate $Q_{\mathcal{S}_0, \mathcal{S}_1}$:

$$Q_{\mathcal{S}_0, \mathcal{S}_1} \triangleq \frac{\mathcal{F}\{\mathcal{S}_0\}^* \cdot \mathcal{F}\{\mathcal{S}_1\}}{|\mathcal{F}\{\mathcal{S}_0\}| \cdot |\mathcal{F}\{\mathcal{S}_1\}|} \quad (1)$$

on the basis that if space is sampled sufficiently densely, for $k, \xi \in \mathbb{Z}: k, \xi \in [0, N_s - 1]$:

$$\begin{aligned} \mathcal{S}_0[k] &\simeq \mathcal{S}_1[(k - \xi) \bmod N_s] \Leftrightarrow \\ \mathcal{F}\{\mathcal{S}_0\}(u) &\simeq e^{-j2\pi\xi u/N_s} \cdot \mathcal{F}\{\mathcal{S}_1\}(u) \end{aligned}$$

and, therefore, since $2\pi \frac{\xi}{N_s} = \xi\gamma$: $Q_{\mathcal{S}_0, \mathcal{S}_1}(u) \simeq e^{-j\xi\gamma u}$.

The inverse of $Q_{\mathcal{S}_0, \mathcal{S}_1}$ is a Kronecker δ -function $q_{\mathcal{S}_0, \mathcal{S}_1} = \mathcal{F}^{-1}\{Q_{\mathcal{S}_0, \mathcal{S}_1}\}$ centered at $\xi = \arg \max q_{\mathcal{S}_0, \mathcal{S}_1}(u)$. If the difference in orientation between the two scans is $\Delta\theta$, then $\Delta\theta = \xi\gamma + \delta\theta$, where $\bmod(|\delta\theta|, \gamma) = \lambda \in [0, \frac{\gamma}{2}]$. Therefore for a given number of emitted rays N_s there remains an unresolved orientation error $|\delta\theta| \leq \gamma/2$. The contribution of this error to the scan-matching error is two-fold, as its existence is also propagated to the location estimation method. A method for further reduction of the orientation error is presented in the following.

Let \mathcal{S}_0 be projected onto the $x-y$ plane around an arbitrary but fixed pose $s(x_s, y_s, \theta_s)$, producing point-set M_R . M_R will hereafter be referred to as the map. Then compute 2^ν map-scans (def. II) \mathcal{S}_0^k , $k = 0, \dots, 2^\nu - 1$, starting from orientation θ_s , at $\gamma/2^\nu$ angular increments. Then the orientation estimation process is carried out once between \mathcal{S}_1 and map scan \mathcal{S}_0^k taken from orientation $\theta_0^k = \theta_s + k \cdot \gamma/2^\nu$, for a total of 2^ν times. An alignment metric between the k -th map scan \mathcal{S}_0^k and scan \mathcal{S}_1 is computed according to

$$\text{PD}_k = \frac{2 \max q_{\mathcal{S}_0^k, \mathcal{S}_1}}{\max q_{\mathcal{S}_0^k, \mathcal{S}_0^k} + \max q_{\mathcal{S}_1, \mathcal{S}_1}} \quad (2)$$

The Percent Discrimination metric $\text{PD}_k \in [0, 1]$, and is proportional to the degree of alignment between map-scan

\mathcal{S}_0^k and scan \mathcal{S}_1 , across all 2^ν map-scans \mathcal{S}_0^k . The above analysis is the equivalent of the 2D Fourier-Mellin Invariant matching in one dimension [28].

Let now K denote the index of the k -th map scan \mathcal{S}_0^K scoring the highest PD_K : $\text{PD}_K = \max\{\text{PD}_k\}$, $k = 0, \dots, 2^\nu - 1$. Let also Ξ denote the integer multiple of angle increments γ by which \mathcal{S}_V^K should be rotated counter-clockwise in order to achieve PD_K : $\Xi = \arg \max q_{\mathcal{S}_0^K, \mathcal{S}_1}$. Then the sensor's orientation difference becomes $\Delta\theta = \Xi\gamma + K \cdot \gamma/2^\nu + \delta\theta'$.

If map-scans \mathcal{S}_V^K were computed by raycasting the map of the environment instead of M_R then the residual and unresolved orientation error $|\delta\theta'| \in [0, \gamma/2^{1+\nu}]$. In this case, however, M_R is an approximation of the environment's map in the locality of p_0 . Depending on the magnitude of the sensor's angle increment and the arbitrariness of the environment, this approximation may be viewed as induced local perturbations in the map of the environment. This holds true in the general case as well, where \mathcal{S}_0 and \mathcal{S}_1 are captured from different locations. Therefore attaining $|\delta\theta'| \leq \gamma/2^{1+\nu}$ may not always be possible for all combinations of environments and sensor angle increments.

B. Estimation of Relative Location

Let the assumptions of Problem I hold. Assume now that \mathcal{S}_0 and \mathcal{S}_1 were captured from different positions in the same environment but with the same orientation relative to a fixed reference frame. Let \mathcal{S}_0 be projected onto the $x-y$ plane around pose $s(0, 0, 0)$, producing point-set M_L . Assuming that \mathcal{S}_1 was captured in a neighbourhood of \mathcal{S}_0 , then M_L is a perturbed local map of the environment with respect to sensor measurement \mathcal{S}_1 . Aside from measurement noise, this perturbation manifests due to the finiteness of the sensor's angle increment and to the fact that different portions of the environment are perceptible and therefore measurable from different locations [5]. The nature of these perturbations on map-scans captured within M_L is additive and finite. Under these assumptions the problem of (scan-)matching scan \mathcal{S}_1 to scan \mathcal{S}_0 may be transformed into a problem of scan-to-map-scan matching, where the aim is registering scan \mathcal{S}_1 to map M_L : i.e. estimating the pose p_1 from where \mathcal{S}_1 was captured within M_L . Theorem II [30] guarantees that the error of the location estimate between the poses from which the two scans were captured is bounded in a neighbourhood of the origin, if the location component of the pose estimate of p_1 is treated according to Theorem I, when its initial value is set to $\hat{p}_1 = s$.

Theorem I. *Let a panoramic 2D range scan \mathcal{S}_R be captured from a physical range sensor from unknown pose $p = (l, \theta)$, $l = (x, y)$. Let M be the map of the world in which the scan was captured. Let a pose estimate $\hat{p} = (\hat{l}, \hat{\theta})$ reside in the neighbourhood of p in the map's frame of reference. Additionally, let $\hat{\theta} = \theta$. Assume that \mathcal{S}_R is disturbance-free, and that the map of the environment captures the latter perfectly. Then, treating the estimate of the location of the sensor as a state variable $\hat{l}[k] = [\hat{x}[k], \hat{y}[k]]^\top$ and updating*

it according to the difference equation

$$\hat{l}[k+1] = \hat{l}[k] + \mathbf{u}[k] \quad (3)$$

where $\hat{l}[0] = \hat{l} = [\hat{x}, \hat{y}]^\top$, i.e. the supplied initial location estimate,

$$\mathbf{u}[k] = \frac{1}{N_s} \begin{bmatrix} \cos \hat{\theta} & \sin \hat{\theta} \\ \sin \hat{\theta} & -\cos \hat{\theta} \end{bmatrix} \begin{bmatrix} X_{1,r}(\mathcal{S}_R, \mathcal{S}_V | \hat{\mathbf{p}}[k]) \\ X_{1,i}(\mathcal{S}_R, \mathcal{S}_V | \hat{\mathbf{p}}[k]) \end{bmatrix} \quad (4)$$

where $X_{1,r}(\cdot)$ and $X_{1,i}(\cdot)$ are, respectively, the real and imaginary parts of the complex quantity X_1 :

$$\begin{aligned} X_1(\mathcal{S}_R, \mathcal{S}_V | \hat{\mathbf{p}}[k]) &= X_{1,r}(\mathcal{S}_R, \mathcal{S}_V | \hat{\mathbf{p}}[k]) + iX_{1,i}(\mathcal{S}_R, \mathcal{S}_V | \hat{\mathbf{p}}[k]) \\ &= \sum_{n=0}^{N_s-1} (\mathcal{S}_R[n] - \mathcal{S}_V[n]|_{\hat{\mathbf{p}}[k]}) \cdot e^{-i\frac{2\pi n}{N_s}} \end{aligned} \quad (5)$$

where $\mathcal{S}_R[n]$ and $\mathcal{S}_V[n]|_{\hat{\mathbf{p}}[k]}$ are, respectively, the ranges of the n -th ray of real scan \mathcal{S}_R and map-scan $\mathcal{S}_V|_{\hat{\mathbf{p}}[k]}$ captured via raycasting the map M from $\hat{\mathbf{p}}[k] = (\hat{l}[k], \theta)$ —then $\hat{l}[k]$ converges to l uniformly asymptotically as $k \rightarrow \infty$.

Theorem II. Let the assumptions of Theorem I hold. Assume additionally that the ranges of either or both real and virtual range scans \mathcal{S}_R and \mathcal{S}_V are affected by additive, bounded disturbances. Then $\hat{l}[k]$ is uniformly bounded for $k \geq k_0$ and uniformly ultimately bounded in a neighbourhood of l . Its size depends on the suprema of the disturbance corrupting the range measurements of the two scans.

Remark I. Without loss of generality, subsequent to the application of Theorem I, the location error is proportional to the orientation error.

Let $\hat{\mathbf{p}}'_1$ denote the resulting pose estimate of \mathbf{p}_1 in M_L . Then $\hat{T} = \hat{\mathbf{p}}'_1 - s = \hat{\mathbf{p}}'_1$ is the estimate of the 3D rigid transformation of the sensor as it moved from the pose where it captured \mathcal{S}_0 to that where it captured \mathcal{S}_1 .

C. Joint Estimation of Relative Orientation and Location

The previous two sections describe two methods of how it is possible to (a) estimate the relative orientation between two panoramic 2D range scans when both are captured from the same position but from different orientations, and (b) estimate their relative location when both are captured from the same sensor orientation but from different locations. In the general case, however, no equality stands. The following analysis describes how these two methods are combined in tandem in order to solve Problem I.

Let the assumptions of Problem I hold. Then denote by M the point-set that is the result of the projection of range scan \mathcal{S}_0 to the $x-y$ plane around $s(0, 0, 0)$. Then the objective is estimating the pose \mathbf{p}_1 from where \mathcal{S}_1 was captured relative to s by way of registering \mathcal{S}_1 to map M .

Given an input pose estimate $\hat{\mathbf{p}}_1(\hat{x}_1, \hat{y}_1, \hat{\theta}_1)$, range scan \mathcal{S}_1 , the map M , and a sampling degree ν , the One-step Pose Estimation system (fig. 2) first calculates 2^ν pose estimates of \mathbf{p}_1 : $\mathbf{P}_{OC} = \{(\hat{x}_1^k, \hat{y}_1^k, \hat{\theta}_1^k)\}$, $k = 0, \dots, 2^\nu-1$, according to the orientation estimation method described in section IV-A. The initial pose estimate of \mathbf{p}_1 is $\hat{\mathbf{p}}_1 = s$. If scans \mathcal{S}_0 and

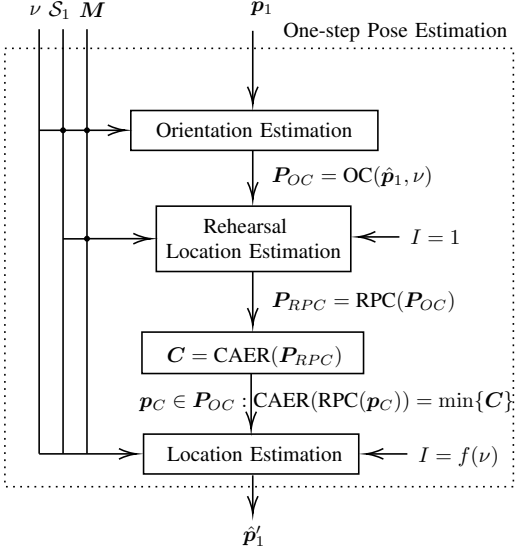


Fig. 2: FSM iteratively invokes the One-step Pose Estimation method. Given a pose estimate of where scan S_1 was captured within M , the method attempts to register S_1 to M by estimating first its relative orientation and then its location with respect to the input pose estimate

S_1 were captured from the same location, then the Percent Discrimination metric (eq. 2) would suffice in serving as an accurate determinant of the orientation of p_1 . In practice, however, the ranking provided by the Percent Discrimination metric is confounded by the incoincidence of the two locations. In order to mitigate this effect, each pose estimate in \mathbf{P}_{OC} is given over to the Position Estimation system, where the position of each pose estimate is displaced once ($I = 1$), according to the method described in section IV-B. This operation produces the pose set $\mathbf{P}_{RPC} = \{(\hat{x}_1^k, \hat{y}_1^k, \hat{\theta}_1^k)\}$, $|\mathbf{P}_{RPC}| = 2^\nu$. The purpose of this operation is for it to provide an advance view of the next step of location estimation: the less rotationally misaligned a pose estimate of p_1 is, the less it will diverge in terms of orientation and hence position with respect to p_1 once inputted to the position estimation system (remark I). This divergence is captured by the Cumulative Absolute Error per Ray (CAER) metric:

$$\text{CAER}_k = \sum_{n=0}^{N_s-1} \left| \mathcal{S}_1[n] - \mathcal{S}_V^k[n] \right|_{(\hat{x}_1^k, \hat{y}_1^k, \hat{\theta}_1^k)} \quad (6)$$

where \mathcal{S}_V^k is the map-scan captured from $(\hat{x}_1^k, \hat{y}_1^k, \hat{\theta}_1^k)$, $k = 0, \dots, 2^\nu-1$, within M . The CAER metric (fig. 3) encodes at the same time a degree of alignment of position and orientation between its two input scans. By rehearsing the position estimation of each pose estimate in \mathbf{P}_{OC} and capturing the CAER for each of its displaced pose estimates in \mathbf{P}_{RPC} , it is possible to establish a pose error rank between pose estimates in \mathbf{P}_{OC} and simultaneously retain only one pose estimate for the next iteration of the One-step Pose Estimation method.¹ The pose estimate $\mathbf{p}_C \in \mathbf{P}_{OC}$ which, when translated once,

¹ Alternatively, correcting the position of 2^ν pose estimates and feeding them back to the One-step Pose Estimation method would incur exponential costs in time of execution.

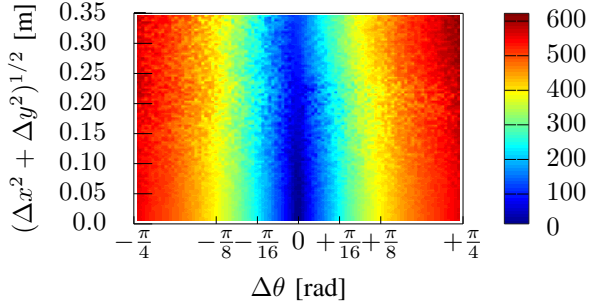


Fig. 3: A profile of the CAER metric (eq. (6)) from 10^6 pairs of sample scans, depending on the distance $(\Delta x^2 + \Delta y^2)^{1/2}$ and relative orientation $\Delta\theta$ of the poses from where the two scans were captured. Pose estimates closer to the true pose in terms of orientation (a) exhibit lower CAER values than those further away from it and (b) produce lower location errors once inputted to the Location Estimation system

records the minimum CAER among all similarly-treated pose estimates in P_{OC} is inputted to the Position Estimation method proper. The number of translation iterations I it undergoes is an increasing function in the degree of map sampling ν . The Position Estimation system produces \hat{p}'_1 , which is then fed back to the Orientation Estimation system in the form of a new pose estimate of p_1 : $\hat{p}_1 \leftarrow \hat{p}'_1$. In practice, the pose set P_{OC} is supplemented with one pose whose location component is equal to \hat{p}_1 and whose orientation is equal to the orientation of p_C that produces the minimum CAER over time. This addition introduces a form of memory to the system, which assists it in avoiding divergence and which, therefore, benefits speed of execution.

Given pose \hat{p}_1 , range scan S_1 , and the map M , the pose estimation method proposed iteratively invokes the One-step Pose Estimation process until a set of termination conditions is met. Denoting the former by FSM (Fourier Scan Matching), FSM starts off with an initial degree of sampling the map $\nu = \nu_{\min}$. The input pose estimate \hat{p}_1 is processed by the One-step Pose Estimation process, and its output \hat{p}'_1 is examined with regard to Recovery and Convergence conditions. If the resulting pose estimate falls outside of the map M then a new pose estimate is generated from the initially supplied pose estimate s , and the process is reset. If no significant pose estimate correction is observed $\|\hat{p}'_1 - \hat{p}_1\|_2 < \varepsilon_{\delta_p}$, then the degree of map sampling ν is increased. Its increase serves as a means of reducing the orientation and hence the position estimate error further. Otherwise, the One-step Pose Estimation process is iterated until a maximum degree of map sampling is reached $\nu = \nu_{\max}$, at which point FSM terminates. Its output is \hat{p}'_1 , which is the pose estimate of p_1 in the frame of reference of M . The roto-translation $\hat{T} = \hat{p}'_1 - s = \hat{p}'_1$ is the estimate of the sensor's true motion T .

V. RESULTS

A. Experimental Design

The experimental procedure was conducted using a collection $D = \{D_k\}, k = 1, \dots, 5$ of five heterogeneous benchmark datasets, courtesy of the Department of Computer Science, University of Freiburg, comprising a total of $|D| = 45402$ scan measurements [31]. For purposes of comparison against state-of-the-art scan-matching methods the experimental procedure is extended to the Normal Distributions Transform (NDT) scan-matching method [25], FastGICP [14] and PLICP \circ GPM [22]. The latter shall be denoted hereafter by the acronym CSM. GPM was used initially in order to overcome the angular realignment problems [22] of PLICP. NDT, FastGICP, and CSM belong to the *established* state-of-the-art methods of scan-matching [21][32]-[36]. In addition, the experimental procedure is extended to FastVG-ICP [21] and NDT-PSO [37].

The experimental setup is the following. The rays of each dataset D instance $D^d = 1, 2, \dots, |D|$ are first projected to the $x - y$ plane around r^d . The dataset's scans are not panoramic, therefore the remaining space is filled with a semicircular arc that joins the scan's two extreme ends. Alternative fashions for closing-off the environment have been found equivalent with respect to the performance of the tested methods. The resulting point-set is regarded as the environment W^d in which the range sensor operates. Then the pose p_0^d from which S_0^d is captured is generated randomly within the polygon formed by W^d . The pose p_1^d from which the sensor captured S_1 is then obtained by perturbing the components of p_0^d with quantities extracted from uniformly distributed error distributions $U_{xy}(-\bar{\delta}_{xy}, \bar{\delta}_{xy})$, $U_\theta(-\bar{\delta}_\theta, \bar{\delta}_\theta)$; $\bar{\delta}_{xy}, \bar{\delta}_\theta \in \mathbb{R}_{\geq 0}$.

Range scans S_0^d and S_1^d are then computed by locating the intersection points between N_s rays emanating from p_0^d and p_1^d , respectively, and the polygon formed by W^d across an angular field of view $\lambda = 2\pi$. The inputs to all algorithms are then set to S_0^d and S_1^d . Their output is $p_1^{d'}$. The roto-translation $\hat{T}^d = p_1^{d'}$ is the estimate of the motion $T^d = p_1^d - p_0^d$ of the range sensor.

For every pose estimate $p_1^{d'}$ outputted by each algorithm, its offset from the actual pose p_1^d is recorded in the form of the orientation error and the 2-norm position error. In order to test for the performance of the proposed method with use of real sensors, five levels of noise acting on the range measurements of the scans are tested. The range measurements are perturbed by zero-mean normally-distributed noise with standard deviation $\sigma_R \in \{0.01, 0.03, 0.05, 0.10, 0.20\}$ m. The values of tested standard deviations were calculated from commercially available panoramic LIDAR scanners by identifying the magnitude of their reported maximum range errors and dividing it by a factor of three. The rationale is that 99.73% of errors are located within 3σ around the actual range between a ray and an obstacle, assuming errors are distributed normally. The minimum standard deviation is reported for VELODYNE sensors [38]; the rest are reported for price-appealing but disturbance-laden RPLIDAR [39] and

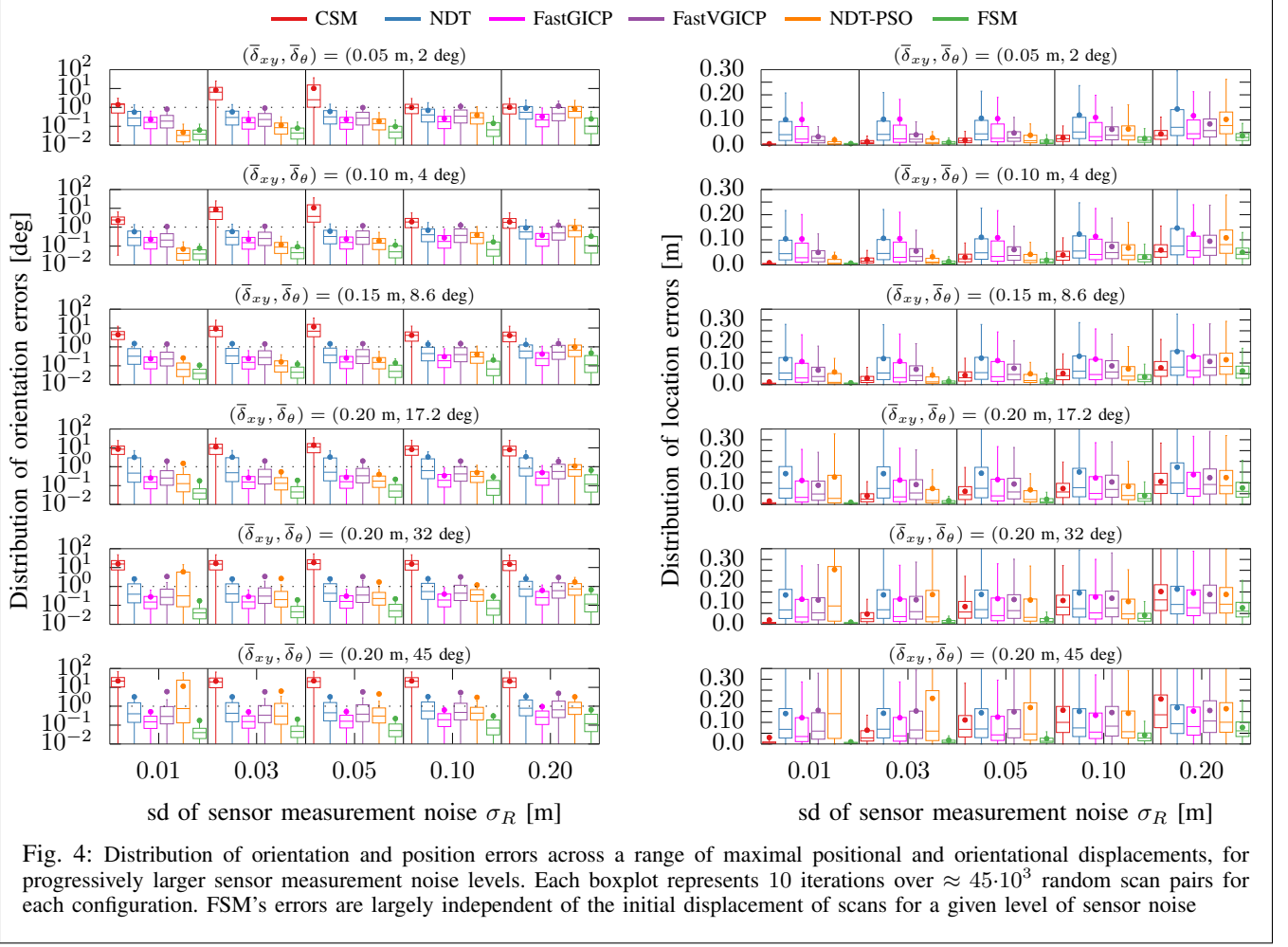


Fig. 4: Distribution of orientation and position errors across a range of maximal positional and orientational displacements, for progressively larger sensor measurement noise levels. Each boxplot represents 10 iterations over $\approx 45 \cdot 10^3$ random scan pairs for each configuration. FSM's errors are largely independent of the initial displacement of scans for a given level of sensor noise

YDLIDAR [40] sensors. The size of the input scans was set to $N_s = 360$ rays. The minimum and maximum map oversampling rates of FSM were set to $(2^{\nu_{\min}}, 2^{\nu_{\max}}) = (2^0, 2^3)$. The number of iterations of the translational component at each map sampling degree ν was set at $I = 5\nu$. The orientation convergence threshold was set to $\varepsilon_{\delta p} = 10e-5$. Maximal displacements $\bar{\delta}_{xy}$ and $\bar{\delta}_\theta$ were chosen as such by prior art tests [22]. For each experiment all algorithms ran for $E = 10$ times across all instances of D . Therefore each method underwent a total of $10 \times 45402 \times 6 \times 5 \sim O(10^8)$ experiments. The orientation and position error distributions reported below are those across all $E \times D$ experiments of the same configuration. All experiments and algorithms were run serially, in C++, on a single thread, on a machine with a CPU frequency of 4.0 GHz. The implementations of CSM, NDT, FastGICP, FastVGICP, and NDT-PSO were taken from [41].

B. Performance

Figure 4 shows the distribution of rotation and translation errors across all experiments for all tested algorithms.

FSM's position and orientation errors are equal to or lower than the most accurate method for each displacement

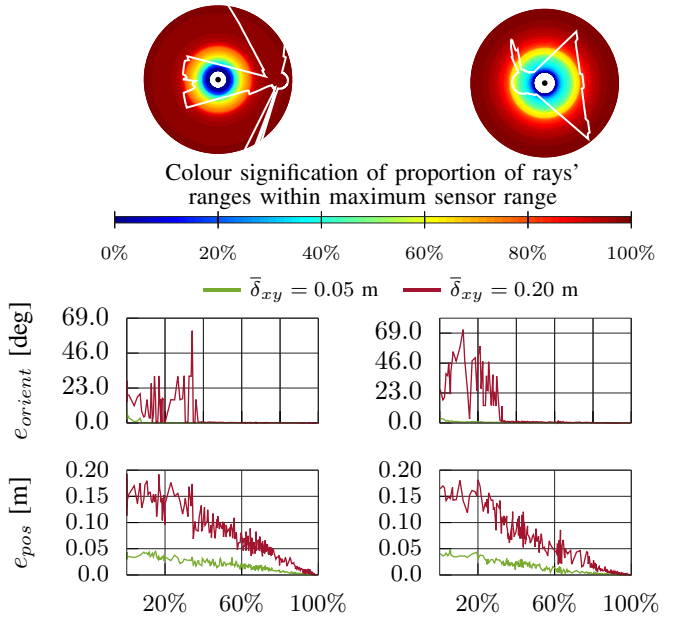


Fig. 5: FSM's performance with respect to receding maximum range

and sensor noise configuration. As displacements and sensor noise levels increase, its errors increase at a lower rate than any tested method. The magnitude of FSM's errors is largely independent of the displacement of the two input scans for a given level of sensor noise (fig. 1). The juxtaposition of the six methods' errors at high levels of sensor noise highlight the robustness afforded to FSM by the Discrete Fourier transform and its properties.

In terms of execution time, CSM ranged between 4.8-17.5 ms, NDT 8.1-19.9 ms, FastGICP 3-9 ms, FastVGICP 3.8-6.8 ms, NDT-PSO 190-200 ms, and FSM between 13.2 and 16.7 ms. The measurement frequency of modern LIDAR sensors ranges from 12-20 Hz; therefore FSM runs in real time in modern processors.

VI. CONCLUSIONS AND FUTURE STEPS

This paper has presented a scan-matching method for panoramic LIDAR sensors. The approach rests on properties of the DFT, which afford it increased robustness and accuracy compared to established scan-matching approaches in the face of measurement noise exhibited by real-life sensors. The C++ code of the proposed method, along with the implementation of the conducted experiments is available at <https://github.com/l19i/fsm>.

REFERENCES

- [1] Ju, X., Xu, D., Zhao, X., Yao, W., & Zhao, H. (2019). "Learning Scene Adaptive Covariance Error Model of LiDAR Scan Matching for Fusion Based Localization". 2019 IEEE Intelligent Vehicles Symposium (IV), 1789-1796.
- [2] N. Kumar and Z. Vamossy, "Laser Scan Matching in Robot Navigation", 2018 IEEE 12th International Symposium on Applied Computational Intelligence and Informatics (SACI), Timisoara, 2018, pp. 000241-000246, doi: 10.1109/SACI.2018.8440969.
- [3] H. Zhang, N. Chen, G. Fan and D. Yang, "An improved scan matching algorithm in SLAM," 2019 6th International Conference on Systems and Informatics (ICSAI), Shanghai, China, 2019, pp. 160-164, doi: 10.1109/ICSAI48974.2019.9010259.
- [4] E. Pedrosa, A. Pereira and N. Lau, "Fast Grid SLAM Based on Particle Filter with Scan Matching and Multithreading," 2020 IEEE International Conference on Autonomous Robot Systems and Competitions (ICARSC), Ponta Delgada, Portugal, 2020, pp. 194-199, doi: 10.1109/ICARSC49921.2020.9096191.
- [5] E. B. Olson, "Real-time correlative scan matching," 2009 IEEE International Conference on Robotics and Automation, Kobe, Japan, 2009, pp. 4387-4393, doi: 10.1109/ROBOT.2009.5152375.
- [6] Zhang, Shuaipeng & Xiao, Liang & Nie, Yiming & Dai, Bin & Hu, Chaofang. (2020). "Lidar Odometry and Mapping Based on Two-stage Feature Extraction". 3966-3971. 10.23919/CCC50068.2020.9188810.
- [7] Cooper, M.A.; Raquet, J.F.; Patton, R. Range Information Characterization of the Hokuyo UST-20LX LIDAR Sensor. *Photonics* 2018, 5, 12.
- [8] Lu, Feng and Miliios, Evangelos, "Robot Pose Estimation in Unknown Environments by Matching 2D Range Scans", *Journal of Intelligent and Robotic Systems*, volume 18, number 3, pp. 249-275, 1997, doi 10.1023/A:1007957421070, ISSN 1573-0409
- [9] P. J. Besl and N. D. McKay, "A method for registration of 3-D shapes", *IEEE Transactions on Pattern Analysis and Machine Intelligence*, 1992, volume 14, number 2, pp. 239-256, doi 10.1109/34.121791, ISSN 0162-8828
- [10] S. T. Pfister, K. L. Kriegbaum, S. I. Roumeliotis and J. W. Burdick, "Weighted range sensor matching algorithms for mobile robot displacement estimation," Proceedings 2002 IEEE International Conference on Robotics and Automation (Cat. No.02CH37292), Volume 2, Washington, DC, USA, 2002, pp. 1667-1674, doi: 10.1109/ROBOT.2002.1014782
- [11] D. Chetverikov, D. Svirko, D. Stepanov and P. Krsek, "The Trimmed Iterative Closest Point algorithm," Object recognition supported by user interaction for service robots, Quebec City, Quebec, Canada, 2002, pp. 545-548 Volume 3, doi: 10.1109/ICPR.2002.1047997
- [12] J. Minguez, F. Lamiraux and L. Montesano, "Metric-Based Scan Matching Algorithms for Mobile Robot Displacement Estimation," Proceedings of the 2005 IEEE International Conference on Robotics and Automation, Barcelona, Spain, 2005, pp. 3557-3563, doi: 10.1109/ROBOT.2005.1570661
- [13] Martinez, Jorge & Gonzalez-Jimenez, Javier & Morales, J. & Mandow, Anthony & Garcia, Alfonso. (2006). "Mobile robot motion estimation by 2D scan matching with genetic and iterative closest point algorithms". *Journal of Field Robotics*. 23. 21-34. 10.1002/rob.20104.
- [14] A. Segal, D. Hahnel and S. Thrun "Generalized-ICP". Proc. of Robotics: Science and Systems. 10.15607/RSS.2009.V.021., 2009
- [15] Wang, J. Zhao, M. Chen, W. "MIM-SLAM: A Multi-Level ICP Matching Method for Mobile Robot in Large-Scale and Sparse Scenes". *Appl. Sci.* 2018, 8, 2432.
- [16] Tian, Yingzhong; Liu, Xining; Li, Long; Wang, Wenbin. 2019. "Intensity-Assisted ICP for Fast Registration of 2D-LIDAR" *Sensors* 19, no. 9: 2124.
- [17] Naus, Krzysztof; Marchel, ukasz. 2019. "Use of a Weighted ICP Algorithm to Precisely Determine USV Movement Parameters" *Appl. Sci.* 9, no. 17: 3530.
- [18] Linh Tao, Tam Bui, Toshio Ito, "MODIFIED ITERATIVE CLOSEST POINT MATCHING FOR 2D LIDAR LASER DATA", 14th South East Asian Technical University Consortium 2020 (SEATUC 2020) 27th 28th February 2020, KX Building, KMUTT, Bangkok, Thailand
- [19] Huchao Xu, Letao Zhou, Yinghao Zhao, Zheng Yuan, " A Two-Dimensional Point Cloud Matching Method Based on ICP Improvement", China Satellite Navigation Conference (CSNC) 2020 Proceedings: Volume I pp 390-398
- [20] Marchel, .; Specht, C.; Specht, M. "Testing the Accuracy of the Modified ICP Algorithm with Multimodal Weighting Factors". *Energies* 2020, 13, 5939. <https://doi.org/10.3390/en13225939>
- [21] K. Koide, M. Yokozuka, S. Oishi and A. Banno, "Voxelized GICP for Fast and Accurate 3D Point Cloud Registration," 2021 IEEE International Conference on Robotics and Automation (ICRA), 2021, pp. 11054-11059, doi: 10.1109/ICRA48506.2021.9560835.
- [22] A. Censi, "An ICP variant using a point-to-line metric," 2008 IEEE International Conference on Robotics and Automation, Pasadena, CA, 2008, pp. 19-25, doi: 10.1109/ROBOT.2008.4543181.
- [23] F.A. Donoso, K.J. Austin, P.R. McAree, "How do ICP variants perform when used for scan matching terrain point clouds?", *Robotics and Autonomous Systems*, Volume 87, 2017, Pages 147-161, ISSN 0921-8890, <https://doi.org/10.1016/j.robot.2016.10.011>.
- [24] A. Censi, "Scan matching in a probabilistic framework," Proceedings 2006 IEEE International Conference on Robotics and Automation, 2006. ICRA 2006., Orlando, FL, 2006, pp. 2291-2296, doi: 10.1109/ROBOT.2006.1642044.
- [25] P. Biber and W. Strasser, "The normal distributions transform: a new approach to laser scan matching," Proceedings 2003 IEEE/RSJ International Conference on Intelligent Robots and Systems (IROS 2003) (Cat. No.03CH37453), Las Vegas, NV, USA, 2003, pp. 2743-2748, Volume 3, doi: 10.1109/IROS.2003.1249285
- [26] Yu, Heng & Zeng, Yadan & Dai, Houde. (2018). "A Novel Scan Matching Method for Mobile Robot Based on Phase Only Matched Filtering", 391-394. 10.1109/ICInfA.2018.8812336.
- [27] Jiang, Guolai & Lei, Yin & Liu, Guodong & Xi, Weinan & Ou, Yongsheng. (2018). "FFT-Based Scan-Matching for SLAM Applications with Low-Cost Laser Range Finders". *Applied Sciences*. 9. 41. 10.3390/app9010041.
- [28] Qin-Sheng Chen, M. Deruise and F. Deconinck, "Symmetric phase-only matched filtering of Fourier-Mellin transforms for image registration and recognition," in *IEEE Transactions on Pattern Analysis and Machine Intelligence*, vol. 16, no. 12, pp. 1156-1168, Dec. 1994, doi: 10.1109/34.387491.
- [29] Filotheou, A., Tsardoulas, E., Dimitriou, A. et al. "Pose Selection and Feedback Methods in Tandem Combinations of Particle Filters with Scan-Matching for 2D Mobile Robot Localisation". *J Intell Robot Syst* 100, 925944 (2020). <https://doi.org/10.1007/s10846-020-01253-6>
- [30] A. Filotheou, "Correspondenceless scan-to-map-scan matching of homorianted 2D scans for mobile robot localisation", *Robotics and Autonomous Systems*, vol. 149, 2022, <https://doi.org/10.1016/j.robot.2021.103957>

- [31] The datasets are available at <http://ais.informatik.uni-freiburg.de/slamevaluation/datasets.php>; last accessed 25 Jan 2022
- [32] P. Xu, F. Gu, Z. Song and J. Li, "Non-iterative multiple data registration method based on the motion screw theory and trackable features," 2018 24th International Conference on Pattern Recognition (ICPR), 2018, pp. 2428-2432, doi: 10.1109/ICPR.2018.8545473.
- [33] H. Sobreira, C. Costa, I. Sousa, L. Rocha, J. Lima, P. Farias, P. Costa, and A. Moreira, "Map-Matching Algorithms for Robot Self-Localization: A Comparison Between Perfect Match, Iterative Closest Point and Normal Distributions Transform.", 2019, Journal of Intelligent and Robotic Systems. 93. 10.1007/s10846-017-0765-5.
- [34] A. Pishehvari, U. Iurgel, S. Lessmann, L. Roese-Koerner and B. Tibken, "Radar Scan Matching Using Navigation Maps," 2019 Third IEEE International Conference on Robotic Computing (IRC), 2019, pp. 204-211, doi: 10.1109/IRC.2019.00038.
- [35] W. Qingshan and Z. Jun, "Point Cloud Registration Algorithm Based on Combination of NDT and PLICP," 2019 15th International Conference on Computational Intelligence and Security (CIS), 2019, pp. 132-136, doi: 10.1109/CIS.2019.00036.
- [36] Q. -H. Pham, N. -H. Tran, T. -T. Nguyen and T. -P. Tran, "Online Robust Sliding-Windowed LiDAR SLAM in Natural Environments," 2021 International Symposium on Electrical and Electronics Engineering (ISEE), 2021, pp. 172-177, doi: 10.1109/ISEE51682.2021.9418728.
- [37] S. Bouraine, A. Bougouffa and O. Azouaoui, "NDT-PSO, a New NDT based SLAM Approach using Particle Swarm Optimization," 2020 16th International Conference on Control, Automation, Robotics and Vision (ICARCV), 2020, pp. 321-326, doi: 10.1109/ICARCV50220.2020.9305519.
- [38] VELODYNE sensors' datasheet <https://visimind.com/wp-content/uploads/2018/12/LiDAR-Product-Brochure.pdf>, last accessed 24 Mar 2021
- [39] RPLIDAR A2M8 datasheet https://cdn.sparkfun.com/assets/e/a/f/9/8/LD208_SLAMTEC_rplidar_datasheet_A2M8_v1.0_en.pdf, last accessed 24 Mar 2021
- [40] YDLIDAR datasheets <https://www.manualshelf.com/brand/ydlidar>, last accessed 24 Jan 2022
- [41] Link to repositories for implementation of CSM, NDT, FastG-ICP, FastVGICP, and NDT-PSO: <https://gist.github.com/li9i/c159e282ce5a5ef34500b26c34499c08>